Perspective: Structural dynamics in condensed matter mapped by femtosecond x-ray diffraction

T. Elsaesser and M. Woerner

Citation: The Journal of Chemical Physics **140**, 020901 (2014); doi: 10.1063/1.4855115
View online: http://dx.doi.org/10.1063/1.4855115
View Table of Contents: http://scitation.aip.org/content/aip/journal/jcp/140/2?ver=pdfcov
Published by the AIP Publishing

Perspective: Structural dynamics in condensed matter mapped by femtosecond x-ray diffraction

T. Elsaesser and M. Woerner
Max-Born-Institut für Nichtlineare Optik und Kurzzeitspektroskopie, 12489 Berlin, Germany

(Received 14 October 2013; accepted 6 December 2013; published online 8 January 2014)

Ultrashort soft and hard x-ray pulses are sensitive probes of structural dynamics on the picometer length and femtosecond time scales of electronic and atomic motions. Recent progress in generating such pulses has initiated new directions of condensed matter research, exploiting a variety of x-ray absorption, scattering, and diffraction methods to probe photoinduced structural dynamics. Atomic motion, changes of local structure and long-range order, as well as correlated electron motion and charge transfer have been resolved in space and time, providing a most direct access to the physical mechanisms and interactions driving reversible and irreversible changes of structure. This perspective combines an overview of recent advances in femtosecond x-ray diffraction with a discussion on ongoing and future developments. [http://dx.doi.org/10.1063/1.4855115]

I. INTRODUCTION

Numerous nonequilibrium processes in condensed matter involve changes of atomic and electronic structure. The rearrangement of atoms in a phase transition or in a chemical reaction, charge relocations and changes of spin states in electron transfer and/or magnetic processes, as well as field-driven changes and mixing of electronic orbitals are among the most basic phenomena which determine functional properties. The elementary steps of many of such processes occur in the atto- to femtosecond time domain and have – in part – been addressed by ultrafast spectroscopy in a wavelength range from the far-infrared up to the extreme ultraviolet.[1] Such nonlinear time resolved methods probe the transient dielectric function of the material, including nonlinear contributions up to – in principle – arbitrary order in the electric field of the driving pulse. This approach has revealed ultrafast nonequilibrium dynamics in great detail while insight into transient structures remains indirect and requires to theoretically model the relationship between structure and dielectric function. Thus, probes offering a (sub)atomic spatial and an ultrafast time resolution are required for direct structure mapping.

In recent years, there has been impressive progress in developing and applying novel probes of ultrafast structural dynamics.[2–8] Femtosecond electron scattering and diffraction[5,6] as well as a range of ultrafast x-ray probes[2–4,7] have provided key insight into structure changes underlying physical and chemical processes. This exciting field relies on new technologies to generate and characterize femtosecond electron and x-ray pulses which are synchronized with optical sources and allow for the implementation of pump-probe methods. Early work in this field has mainly focused on optically induced atomic motions, including the spatial propagation of phonons in the excited material, and changes of atomic arrangements, e.g., in irreversible phase transitions such as nonthermal melting. The subsequent substantial improvement of experimental sensitivity has allowed for addressing subtle fully reversible structure changes. In parallel, novel femtosecond x-ray absorption and diffraction methods have grasped transient electron density maps and changes of magnetic structure most directly.

In this article, we present a perspective on recent x-ray diffraction work addressing reversible structural dynamics in condensed matter. The current state of the art in femtosecond x-ray generation, diffraction methods, and recent x-ray diffraction studies of single crystals and polycrystalline matter are discussed. Reviews of early x-ray diffraction work have been presented in Refs. 2–4 and 9–11. Research on diluted gas phase systems and applications of ultrashort x-ray pulses which aim at determining static structure such as single-pulse nanocrystallography[12,13] are not covered here but have partly been discussed in recent reviews.[7,8] The text is organized as follows. In Sec. II, we briefly discuss the present sources of femtosecond x-ray pulses and experimental methods applied in ultrafast x-ray diffraction. Section III covers recent results on real-space atomic motions, spatially and temporally resolved charge density maps, and correlated lattice, charge, and spin dynamics. Conclusions and an outlook on future directions are presented in Sec. IV.

II. SOURCES OF ULTRASHORT X-RAY PULSES AND EXPERIMENTAL METHODS

A. Sources of femtosecond x-ray pulses

There are two different classes of sources of ultrashort x-ray pulses: (i) accelerator based large scale facilities such as free electron lasers (FELs) and so-called slicing beamlines at synchrotrons, and (ii) laser-driven table-top plasma sources. In this section, we present a short summary of the present state of technology.

TABLE I. Femtosecond x-ray sources. Pulse parameters are summarized for the hard x-ray output of LCLS at SLAC, the slicing beamline at the Swiss Light Source (SLS), and laser-driven Cu and Mo Kα plasma sources at the Max Born Institute (MBI) in Berlin.

	FEL (LCLS)	Slicing (SLS)	Laser plasma (MBI)
Photon energy E (keV)	2.0–9.6	4.2–14.0	8.04, 17.48
Bandwidth $\Delta E/E$	$(2–5) \times 10^{-3}$	$\geq 10^{-2}$	2.5×10^{-4}
Photons/s (total)	2.5×10^{14}	2×10^{6}	5×10^{10}, 8×10^{9}
(on sample)			5×10^{6}, 8×10^{5}
Repetition rate (kHz)	0.12	2.0	1.0
Pulse duration (fs)	10–250	100	100
Timing jitter r.m.s. (fs)	200	<100	<100

The present generation of FELs is based on the self-amplified stimulated emission (SASE) of x-rays generated by relativistic electron bunches in undulator structures.[14] X-ray generation starts with spontaneous radiation emitted by an electron bunch (macro-bunch) which is structured into micro-bunches by interaction with the electromagnetic radiation field after a sufficient propagation length in the undulator. As the micro-bunches display a spatial periodicity identical to the light wave, one generates a coherent superposition of the emission from all micro-bunches with an intensity proportional to N^2 where N is the total number of radiating electrons.

The first soft x-ray FEL based on the SASE concept has been FLASH in Hamburg,[15] meanwhile complemented by other facilities worldwide. The first hard x-ray FEL has been the Linac Coherent Light Source (LCLS) at SLAC, Stanford,[16] followed by the SACLA system at Sayo, Japan[17] and a number of ongoing projects, among them XFEL at Hamburg and the SwissFEL at the Paul Scherrer Institute in Villigen. The LCLS peak brightness reaches values of the order of 10^{33} photons/(s mrad^2 mm^2 (0.1% bandwidth)) which is some 8 orders of magnitude higher than in storage ring based synchrotrons. Some key parameters of the LCLS hard x-ray output are summarized in Table I.

The statistically fluctuating initial condition of the SASE process results in fluctuations of both the spectral and the time structure of the generated pulses. The spectral fluctuations[18] are an issue in measurements of x-ray absorption spectra and resonant light-matter interaction schemes, requiring the combined use of x-ray monochromators and normalization methods. The time structure of the SASE FEL pulses consists of a sequence of up to several 100 short coherent spikes. A coherence time of 0.55 fs and a coherence length of 17 μm have been estimated from recent interference experiments.[19] The jitter between the SASE FEL pulses and an external femtosecond laser is of the order of 200 fs r.m.s. (root mean square), affecting the time resolution of optical pump/x-ray probe experiments when averaging over many pump-probe events. Recent progress in addressing this problem will be discussed in Sec. II B.

The spectral and temporal pulse characteristics can be dramatically improved by seeding the FEL, i.e., providing a well-defined initial condition for the amplification process. Very recently, hard x-ray self seeding of the LCLS by a pulse selected in a Bragg monochromator has reduced the spectral bandwidth to 0.5 eV, a factor of 50 less than in un-seeded SASE operation.[20] In the extreme ultraviolet, a high harmonics seed pulse generated with an external laser has been used in the FERMI FEL source at Trieste.[21]

Synchrotron sources based on electron storage rings routinely provide soft or hard x-ray pulses with a duration of the order of 50 ps. Femtosecond pulses have been generated by the so-called beam slicing method[22–24] in which an electron bunch interacts with an intense femtosecond laser pulse in a wiggler or undulator structure, in this way changing the kinetic energy of an ultrashort slice of the much longer electron bunch. The slice modified in energy is spatially separated from the main bunch and generates an ultrashort x-ray pulse in an undulator. This scheme works at kilohertz repetition rates determined by the laser system and offers a time resolution of approximately 100 fs in optical pump/x-ray probe experiments. In Table I, we summarize parameters of the FEMTO beam line at the Swiss Light Source.[24] The x-ray flux at a photon energy of 5 keV has a value of 4×10^5 photons/(s 0.1% bandwidth), the resulting brightness depends on the focusing conditions in the particular experiment.

Plasma sources rely on the interaction of femtosecond laser pulses with a peak intensity of the order of $I = 10^{17}$ W/cm^2 with a thin metallic target.[25–31] The strong electric field of the pulse extracts electrons from the metal surface by field ionization. The generated free electrons are subsequently accelerated for a half cycle of the driving field into the vacuum, a process called vacuum heating,[27] and in the next half cycle of opposite sign smashed back into the target. The electrons reach a kinetic energy of several hundreds of keV which is proportional to $I\lambda^2$ (λ: wavelength of the driving field). They generate characteristic x-ray emission by inner shell ionization of target atoms and Bremsstrahlung by inelastic scattering within the dense array of target atoms. The time structure of the characteristic x-ray emission is determined by the duration of the driving laser pulse and the electron deceleration kinetics in the target, in particular by the target thickness.

The most advanced hard x-ray plasma sources are driven by sub-50 fs pulses of millijoule energies from amplified Ti:sapphire lasers working at a 1 kHz repetition rate.[30,31] Using Cu tape targets of 20 μm thickness, characteristic Kα pulses at a photon energy of 8.04 keV have been generated with a total flux of up to 5×10^{10} photons/s into the full solid angle. The source diameter of 10 to 15 μm is determined by the laser spot size on the target. The metal tape moves with a speed of several cm/s in order to offer a fresh target volume for subsequent laser pulses with a 1 ms separation in time. The peak brightness of this source emitting in the full solid angle is of the order of 3×10^{17} photons/(s mrad^2 mm^2 (0.1% bandwidth)). For diffraction experiments, x-ray emission into a fraction of several 10^{-4} of the total solid angle is collected with an x-ray optics and focused onto the sample, resulting in a collimated hard x-ray flux of up to several 10^6 photons/s. The duration of the hard x-ray pulses is 100 fs for a target thickness of 20 μm. A major advantage of this generation scheme consists in the synchronization of the x-ray pulses with the driving laser output, the timing jitter is negligible compared to the x-ray pulse duration. Table I summarizes the

main parameters of this source which has been applied in numerous femtosecond diffraction experiments.

An enhancement of the kinetic energy of electrons undergoing the vacuum heating process results in a higher yield of both characteristic x-ray emission and Bremsstrahlung. Here, driver pulses of longer wavelengths and, thus, a longer electron acceleration period are of particular interest. Theoretical simulations suggest a 100-fold increase of the characteristic x-ray flux up to 10^{13} photons/s (10^{10} per pulse) when driving a Cu target of 20 μm thickness by sub-50 fs pulses of a peak intensity of $I = 10^{17}$ W/cm^2 at a center wavelength of $\lambda = 5$ μm. The development of mid-infrared drivers with such output parameters is presently underway.

B. X-ray probes of ultrafast structural dynamics

Most studies of ultrafast structural dynamics make use of a pump-probe approach. A femtosecond optical excitation pulse induces a change of equilibrium structure and an ultrashort x-ray probe pulse of variable time delay maps the momentary structure of the excited sample. Resonant absorption of the pump pulse generates nonequilibrium populations of electronically and/or vibrationally excited states from which a structure changing process starts. Both excitations localized within a unit cell and delocalized electronic or propagating phonon excitations have been generated in this way. For localized excitations, the fraction of excited unit cells in crystalline samples is typically less than 1%. Interaction with nonresonant pump pulses induces a field-driven change and, thus, mixing of quantum states, i.e., a virtual excitation connected with a structural change. In the probing step, interaction with the x-ray pulse should be in the linear regime of light-matter interaction and leave the momentary structure unchanged.

The time resolution of pump-probe experiments is determined by the duration of pump and probe pulses, the timing jitter between them, and the interaction geometry with the sample. Laser-based experiments in which both optical pump and x-ray probe are derived from the output of a single laser system, as well as laser-driven slicing schemes at synchrotrons offer a timing jitter that is negligible compared to the respective pulse durations. A time resolution of the order of 100 fs has been demonstrated with both types of experiments. This issue is more critical when using FELs and an independent laser system for optical excitation. Here, the typical jitter has been of the order of 200 fs when averaging over many pump-probe events. Both the electron bunch timing[32,33] and the optical pump/x-ray probe jitter[34–38] have been studied at different soft and hard x-ray FEL sources and schemes for measuring shot-to-shot timing fluctuations have been presented. Very recently, a sorting scheme for individual pump-probe events has been demonstrated at LCLS which is based on a simultaneous spectral and spatial encoding of pump-induced transmission changes of Si_3N_4 membranes.[38] The correlation of the two independent measurements allows for shrinking the timing uncertainty to approximately 10 fs, close to the x-ray pulse duration.

Ultrafast structural dynamics have been probed via (i) changes of x-ray absorption on inner-shell transitions or x-ray fluorescence of molecular systems in a liquid environment, (ii) nonresonant Bragg diffraction from crystalline materials, i.e., single crystals or polycrystalline powder, and (iii) resonant x-ray diffraction from crystalline materials with a correlated electron and/or spin system, including magnetic systems.

(i) Conceptual and experimental aspects of ultrafast x-ray absorption spectroscopy (XAS) have been reviewed recently.[39–42] Spectrally resolved measurements of both the transient extended x-ray absorption fine structure (EXAFS) and x-ray absorption near-edge structure (XANES) require tunable x-ray probe pulses. Tunable pulses of $\leq$5 eV bandwidth are derived with a monochromator from the output of a slicing beamline or a SASE FEL. The inherent spectral fluctuations of the FEL x-ray pulses lead to strong intensity fluctuations of the frequency selected component, requiring a normalization procedure to extract reliable spectra.[43]

In EXAFS experiments, one probes the absorption continuum above the ionization threshold. In this range, oscillatory features occur due to the interference of the outgoing and rescattered photoelectron waves [Fig. 1(a)]. The EXAFS is dominated by single rescattering events from the nearest neighbors because of the strong damping of the outgoing electron wave by inelastic scattering events. In contrast, the XANES around the absorption edge implies multiple scattering events of the photoelectron [Fig. 1(b)], in this way probing both the atomic arrangement and the electronic structure of the environment. Instead of measuring transient absorption directly, recording the excitation spectra of x-ray

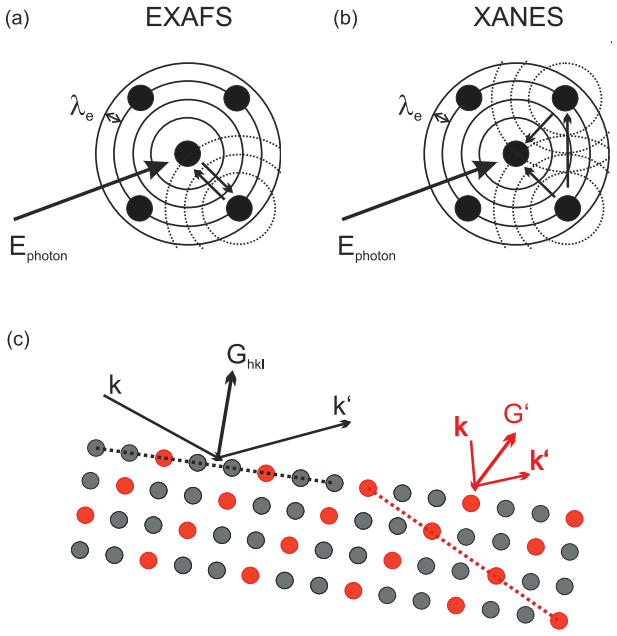

FIG. 1. ((a) and (b)) Schematic of electron scattering processes giving rise to EXAFS and XANES in x-ray absorption. (c) Schematic of x-ray diffraction. Under nonresonant conditions, all atoms contribute to the diffraction signal according to their electron density. In resonant x-ray diffraction (red symbols), the contribution of atoms with an inner-shell transition resonant to the x-ray photon energy is enhanced.

fluorescence provides equivalent information.[43] Ultrafast EXAFS and XAS probe transient local geometries, in particular in liquids and amorphous solids without a long-range order.

(ii) Structural dynamics in photoexcited crystalline matter has been investigated by Bragg diffraction of ultrashort hard x-ray pulses [Fig. 1(c)]. The angular position of a particular Bragg reflection is determined by the condition $\mathbf{k}'-\mathbf{k} = \mathbf{G}_{hkl}$, where $\mathbf{k}'$ and $\mathbf{k}$ are the wavevectors of the scattered and the incoming x-ray pulse and $\mathbf{G}_{hkl}$ is the reciprocal lattice vector of the *hkl* set of lattice planes. The intensity of the Bragg peak $I_{hkl} \propto |F_{hkl}|^2$ is proportional to the square of the structure factor $F_{hkl} = |F_{hkl}|\exp(i\phi_{hkl})$ which represents the (spatial) Fourier transform of the electron density $\rho(\mathbf{r})$ in the unit cell of the crystal. While the time-dependent position of a Bragg peak reflects the time-dependent spacing of lattice planes, its transient intensity gives insight into the redistribution of electronic charge. Time-dependent structure is reconstructed from a sequence of diffraction patterns recorded for different pump-probe delays. Measuring intensity changes on a multitude of Bragg reflections allows for reconstructing time-dependent electron density maps of the excited sample (cf. Sec. III B).

Early work on ultrafast Bragg diffraction has focused on individual or a few Bragg reflections from single crystals for which angular rocking curves and/or diffracted intensities have been measured as a function of pump-probe delay.[2–4,44–50] Recently, the sequential measurement of intensity changes on up to 7 Bragg peaks of Te[51] and the simultaneous detection of changes on several reflections from Bi have been demonstrated, the latter with the help of the femtosecond rotation method for single crystals.[52] Up to 40 reflections have been detected simultaneously with the powder diffraction method for polycrystalline samples,[53–59] implemented with laser-driven plasma sources. Powder diffraction patterns consist of many Debye-Scherrer rings originating from crystallites in the powder with a random orientation of the reciprocal lattice vector $\mathbf{G}_{hkl}$.

Diffraction experiments with accelerator based sources have focused on measuring individual Bragg reflections from single crystal samples so far. Here, the high spatial collimation of the x-ray beams allows for using the major fraction of the x-ray flux for probing.

(iii) Very recently, resonant x-ray diffraction[60] with a femtosecond time resolution has been implemented at LCLS.[61–64] In this method, the elastically scattered x-ray probe pulses are resonant to an atomic inner-shell transition of the system, in most cases in the soft x-ray regime.[60] Under resonance conditions, the diffraction pattern contains – in addition to peaks from nonresonant Bragg diffraction – a resonantly enhanced contribution which can give rise to additional peaks. The resonant atomic scattering factor allows for separating different atomic species with their resonances at different transition energies. This "chemical" sensitivity is particularly attractive when studying materials with large unit cells consisting of many atomic species. In general, resonant atomic scattering factors are tensorial quantities which reflect the ordering of electronic orbitals and the magnetic order of the system. Most of the recent femtosecond experiments have exploited the latter feature in order to determine time-dependent charge and spin order parameters (cf. Sec. III C).

The sensitivity of femtosecond x-ray experiments, i.e., the smallest detectable change of absorption $\Delta A/A_0 = (A(t) - A_0)/A_0$ or diffracted intensity $\Delta I/I_0 = (I(t) - I_0)/I_0$ (A_0, I_0: absorption, diffracted intensity without excitation) depends on the stability of the pulse parameters such as intensity, temporal envelope, pointing stability, and overlap of pump and probe spots on the sample. A fundamental limitation is the photon counting statistics of the x-ray detection process. The counting shot noise leads to a relative uncertainty of $1/\sqrt{N}$ of the detected signal $\Delta A/A_0$ or $\Delta I/I_0$. Counting shot noise is a major issue when using probe pulses with a comparably low x-ray flux from slicing or laser-driven plasma sources. Nevertheless, the so far smallest signals of $\Delta I/I_0 = 10^{-3}$ have been measured with a 100 fs time resolution in powder diffraction experiments with a plasma source working at a 1 kHz repetition rate.[55,56] Typical integration times were several hours per delay position, realized by combining different data sets with a precise relative timing. Future FEL experiments with sufficient beam time at a high x-ray flux should reach a similar sensitivity with much shorter integration times.

III. ULTRAFAST X-RAY DIFFRACTION

A. Real-space atomic motions and vibrational dynamics

Time-resolved x-ray diffraction has been applied to study different regimes of atomic motions. Appropriate optical excitation of a crystalline sample induces local atomic motions in the excited unit cells, typically less than 1% of all unit cells. Such motions have the character of optical phonon wavepackets and occur on a femtosecond time scale determined by the respective phonon frequencies. The related lattice elongations are a few percent of the lattice constant or chemical bond length at most. On a longer time scale, acoustic phonon[65] or polariton[46] propagation has been observed which is equivalent to the propagation of mechanical strain through the material, changing the lattice constants of a much larger fraction of unit cells. Both types of excitations eventually decay via dephasing and energy relaxation of the wavepacket. The population decay into other phonon modes via anharmonic coupling generates a quasi-equilibrium state at an elevated temperature and expands the lattice thermally.

There are different mechanisms for exciting lattice motions which have been reviewed in Ref. 66. In ultrafast x-ray experiments, mostly the following excitation schemes have been applied:[67]

(i) Displacive excitation: Electronic excitation via a bandgap results in a change of the electronic wavefunction and, thus, of the potential energy surface of vibrations/phonons which couple to the electronic transition. The minimum of the excited-state potential is typically shifted along the respective vibrational coordinate, i.e., the initial vibrational wavefunction is displaced with respect to the new minimum. This nonstationary wavepacket moves along the vibrational coordinate, connected with coherent phonon elongations.

(ii) Raman excitation: Impulsive Raman excitation by a broadband femtosecond pulse generates a superposition of optical phonon or polariton eigenstates in the electronic ground state and a concomitant wavepacket motion. Excitation in the range of a dipole-allowed electronic transition enhances the Raman cross section resonantly as has been analyzed in detail in the time-domain wavepacket picture developed in Ref. 68. Coherent phonon generation by stimulated Raman scattering under resonant conditions and the role of the deformation potential in this process have been analyzed in Ref. 69.

(iii) Electronic excitation of metals and semiconductors allows for generating nonequilibrium conduction band electrons which thermalize into a hot (quasi-)Fermi distribution and transfer excess energy to the lattice via electron-phonon coupling. If the fully incoherent cooling process is fast compared to the phonon oscillation period, it can generate an "impulsive" stress that drives coherent motions along low-frequency phonon coordinates. Long-wavelength acoustic excitations which are connected with strain propagation result in changes of the shape and position of the rocking curve.

Local oscillatory lattice motions in real-space are connected with a modulation of electronic charge density and, thus, of the x-ray structure factor. This gives rise to an intensity modulation of the corresponding Bragg peaks. The angular positions of the Bragg peaks remain unaffected as long as the size of the unit cells is unchanged. Phonon frequencies are directly mapped into the oscillation period of Bragg peak intensities whereas the extraction of spatial phonon amplitudes requires a quantitative analysis of the amplitude change of the structure factor. The subsequent decay of the wavepacket and heating of the lattice induce an angular shift of Bragg peaks on time scales between a few and hundreds of picoseconds.

Single crystals or thin crystalline films of Bi have been important model systems for studying coherent lattice motions.[44,49,51,70–74] In the first x-ray diffraction study of displacively excited phonons,[44] oscillations along the A_{1g} optical phonon coordinate of Bi were mapped via intensity oscillations of the (222) and (111) Bragg peaks. The A_{1g} phonon wavepacket modulates the distance between the two basis atoms in the rhomboedric unit cell and a vibrational amplitude of approximately 0.02 nm, roughly 5% of the nearest neighbor distance, has been estimated from the diffraction data.[44] A series of diffraction studies with higher accuracy has allowed for characterizing the coherent A_{1g} phonon motions in great detail.[49,51,71,72] Very recently, coherent elongations of the E_g phonons of Bi which display much smaller amplitudes, have been mapped.[74]

The oscillation frequency of the A_{1g} phonon displays pronounced changes with pump fluence (Fig. 2, Refs. 49 and 70). At a low fluence F < 1 mJ/cm^2, one observes a frequency ν_{1g} close to 2.92 THz, the A_{1g} frequency of the unexcited crystal as determined from Raman studies. With increasing flux, ν_{1g} decreases strongly to about 1/3 of the frequency in the unexcited crystal [Fig. 2(b)]. This behavior reflects a pronounced bond softening. It has been interpreted in terms of approaching a transient ordered state of higher symmetry by eliminating the Peierls distortion which determines the symmetry broken crystal structure of the Bi ground state (A7 symmetry).[70,75]

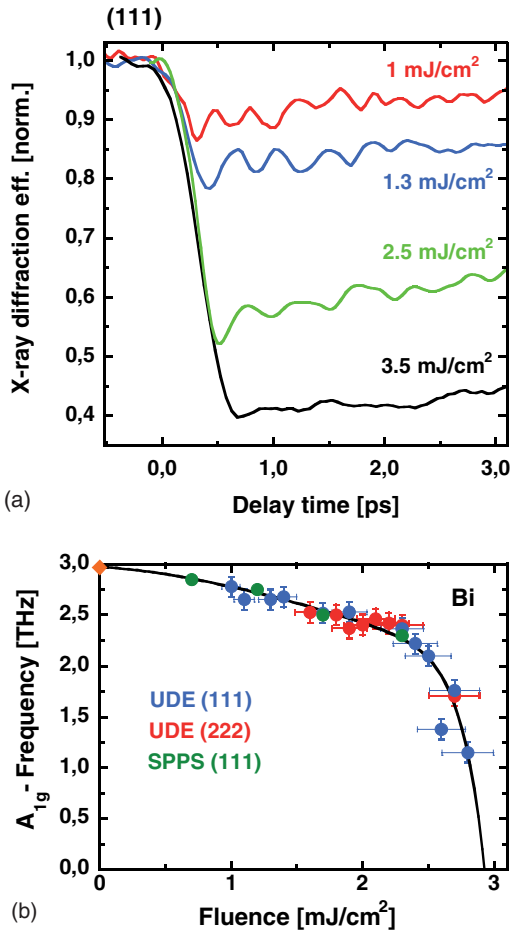

FIG. 2. (a) Optical pump/x-ray probe transients measured with a 50 nm thick Bi film. The oscillations are due to wavepacket motions along the A_{1g} phonon coordinate. (b) Oscillation frequency as a function of excitation fluence. The blue and green symbols were derived from the transient (111) Bragg intensity while the red symbols originate from the (222) reflection. The diamond at 3 THz marks the A1g phonon frequency of unexcited Bi. The decrease of frequency (solid line to guide the eye) reflects a softening of the Bi–Bi bonds upon approaching a phase transition into a state of higher symmetry (solid line). Results taken from Ref. 70.

Nanostructures which consist of a stack of nanometer thick crystalline layers from different materials exhibit an additional type of lattice motion, the so-called superlattice (SL) vibrations. Such modes are connected with elongations along the stack axis c of the layers and change the individual layer thicknesses. The nanometer periodicity d_{SL} of a SL defines a narrow mini-Brillouin zone in k-space, i.e., $-\pi/d_{SL} < k < +\pi/d_{SL}$ [inset of Fig. 3(a)] into which the bulk phonon dispersion along c is back-folded.[76] Driving this system with ultrashort mechanical stress generates a coherent superposition of SL phonon states around q = 0, a wavepacket that modulates the layer thicknesses periodically.

In the x-ray diffraction pattern, the SL periodicity leads to the occurrence of so-called SL diffraction peaks, a regularly spaced series of satellite peaks with a spacing given by $g_{SL} = 2\pi/d_{SL}$. In Fig. 3(a), we show the diffraction pattern

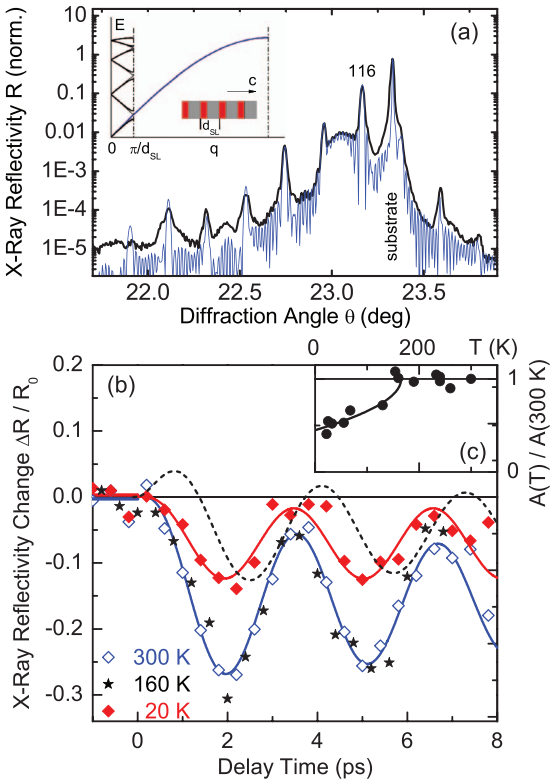

FIG. 3. (a) SRO/STO superlattice diffraction pattern as measured (black solid line) and calculated (blue line) from a dynamical x-ray diffraction theory. The range around the (002) Bragg peak of the bulk STO substrate is shown. Inset: Schematic of the superlattice phonon dispersion in the mini-Brillouin with a boundary at π/d_{SL}. The blue line represents the bulk acoustic phonon dispersion. (b) X-ray reflectivity on the (0 0 116) superlattice diffraction peak as a function of pump-probe delay. Data are shown for the sample in the ferromagnetic (T = 20 K) and paramagnetic (T = 300 K) phase and at the critical temperature T_C = 160 K. Dashed line: Simulation of the response with an instantaneous magnetostrictive and a delayed phonon-mediated stress term. (c) Maximum amplitude of the x-ray reflectivity change (symbols) normalized to its value at T = 300 K as a function of sample temperature. Solid line: Scaled magnetization squared M^2(T) as a function of temperature.

of a $SrRuO_3/SrTiO_3$ (SRO/STO) SL which contains 10 periods of a thickness $d_{SL} = d_{STO} + d_{SRO}$ = 22.72 nm with d_{STO} = 15.24 nm and d_{SRO} = 7.48 nm.[77] The intensity envelope of the SL peak pattern is determined by the structure factors of the SRO and STO unit cells. Launching a coherent SL phonon wavepacket along the *c* axis results in a periodic modulation of the SRO and STO layer thickness, corresponding to a periodic antiphasic expansion and compression of unit cells in adjacent SRO and STO layers at constant d_{SL}. While the angular positions of the SL diffraction peaks remain unchanged, their intensity is strongly modulated due to the angular shift of the SRO and STO envelope functions. This mechanism makes the SL peak intensity a highly sensitive probe of phonon wavepacket motion.

Femtosecond x-ray diffraction experiments have provided detailed insight into the dynamics of semiconductor[45] and perovskite SLs,[77–85] in the latter including ultrafast motions along different anharmonically coupled lattice coordinates.[79] Here, we present results for the ferromagnetic SRO/STO superlattice structure introduced in Fig. 3.[77] Below the Curie temperature T_C = 160 K, SRO exists in a ferromagnetic phase in which the interplay of exchange and kinetic energy of free conduction band electrons leads to an excess population of one spin orientation and, thus, an itinerant ferromagnetic behavior. Above T_C, the material is paramagnetic. In the x-ray diffraction experiments, a 50-fs pump pulse centered at 2.2 μm excited free electrons in the SRO layers (pump fluence 6.5 mJ/cm^2), generating a periodic mechanical stress that induces SL wavepacket motions. The resulting periodic intensity modulation on the (0 0 116) SL peak is mapped by diffracting a hard x-ray probe pulse (Cu Kα at 8.04 keV) from the excited sample. In Fig. 3(b), the diffracted intensity is plotted as a function of pump-probe delay. The large modulation amplitude observed in the paramagnetic phase (sample temperatures 300 and 160 K) is substantially reduced in the ferromagnetic phase while the time evolution of the pump-probe transients remains unchanged. The oscillation period of 3 ps is determined by the layer pair thickness d_{SL} and the velocity of sound. In Fig. 3(c), the x-ray oscillation amplitudes (symbols) from an extended set of data are plotted as a function of sample temperature T.

There are two contributions to the photogenerated stress that drives the observed SL oscillations. At all temperatures, cooling of the photoexcited electrons generates a mechanical stress via a fast population of lattice modes. This term and, thus, the SL oscillations show a delayed onset due to the finite energy transfer time from the electrons to the lattice. The data in Fig. 3(b) suggest a delay between 200 and 700 fs, a more detailed analysis as a function of pump fluence has been presented in Ref. 83. A second stress component originates from magnetostriction, i.e., a change of the lattice dimensions of SRO upon reducing the magnetization by photoexcitation. SRO is known to show a strong magneto-volume effect of negative sign, a reduction of the crystal's volume upon reducing the magnetization. This leads to a stress contribution with a sign opposite to the phonon-mediated stress, reducing the total stress amplitude. Consequently, the amplitude of the SL oscillations is reduced in the ferromagnetic phase. The build-up time of the magnetostrictive stress component is similar to that of the phonon-mediated stress as is evident from the time traces in Fig. 3(b). In particular, an instantaneous onset of magnetostriction (dashed line: simulated kinetics) can be excluded safely. The presence of a magnetostrictive stress component is confirmed by the analysis of the temperature-dependent diffraction amplitudes [Fig. 3(c)] which follow the squared magnetization M^2(T).

Real-space atomic motions and thermal structure changes have also been probed in irreversible phase transitions such as the nonthermal melting of semiconductors and metals.[2–4] Recent experimental and theoretical work has addressed the mechanisms involved in melting of InSb.[86–89]

B. Transient electron density maps

The structure factor $F_{hkl} = |F_{hkl}|\exp(i\phi_{hkl})$ of x-ray diffraction represents the Fourier transform of the electron density $\rho(\mathbf{r})$. This fundamental relation allows for deriving spatially resolved electron density maps from x-ray diffraction patterns containing a large number of Bragg peaks (*hkl*).

Stationary x-ray Bragg and Laue diffraction have widely been applied to generate equilibrium charge density maps with up to picometer spatial resolution.[90,91] The recent implementation of ultrafast x-ray powder diffraction[53] which provides time resolved diffraction patterns consisting of up to 40 Debye-Scherrer rings, has allowed for creating the first transient electron density maps with a time resolution of 100 fs. Such pioneering work has given new insight into field-driven electron relocations[57,58] and the interplay of lattice and electron motions in ionic crystals,[55,56] as well as in elementary chemical processes such as hydrogen transfer.[54]

The change of diffracted intensity $\Delta I_{hkl}(t) = I_{hkl}(t) - I^0_{hkl}$ (I^0_{hkl}: intensity diffracted without excitation) integrated over the Debye-Scherrer ring (*hkl*) is given by

$$\begin{aligned}\Delta I_{hkl}(t) &= M_{hkl} L P_{hkl} \left(|F_{hkl}(t)|^2 - \left|F^0_{hkl}\right|^2\right) \\ &= M_{hkl} L P_{hkl} \left(\left|\eta F^{ex}_{hkl}(t) + (1-\eta) F^0_{hkl}\right|^2 - \left|F^0_{hkl}\right|^2\right).\end{aligned} \tag{1}$$

Here, M_{hkl} is the multiplicity of the (*hkl*) diffraction ring and LP_{hkl} represents the Lorentz polarization factor. F^0_{hkl} and $F^{ex}_{hkl}(t)$ are the structure factors of the unit cell before and after excitation, respectively, and $\eta \ll 1$ is the fraction of excited unit cells. In calculating the quantity $|F_{hkl}(t)|^2$, the product term $F^{ex}_{hkl}(t) \cdot F^0_{hkl}$ describes the interference of x-rays diffracted from excited unit cells with those diffracted from unexcited unit cells. In other words, the strong x-ray component diffracted from unexcited unit cells serves as reference wave in heterodyning the much weaker x-rays diffracted from the small fraction η of modified unit cells.

Deriving electron density maps from the measured intensity changes $\Delta I_{hkl}(t)$ requires to determine $F^{ex}_{hkl}(t)$ in amplitude and phase. For a powder of crystallites consisting of unit cells with an inversion symmetry, the structure of excited crystallites averaged over all orientations in the powder is again inversion-symmetric. Thus, the initial phase $\phi^0_{hkl} = 0, \pi$ is preserved. Neglecting terms of Eq. (1) which are quadratic in η, the following relation between the change in the structure factor $\Delta F_{hkl}(t) = F^{ex}_{hkl}(t) - F^0_{hkl}$ and $\Delta I_{hkl}(t)$ is derived:

$$\eta \Delta F_{hkl}(t) = \eta \left(F^{ex}_{hkl}(t) - F^0_{hkl}\right) = \frac{\Delta I_{hkl}(t)}{2 M_{hkl} L P_{hkl} F^0_{hkl}}. \tag{2}$$

Here, all quantities on the r.h.s. of Eq. (2) are known, allowing for determining $\Delta F_{hkl}(t)$. The latter provide the change $\Delta\rho(\mathbf{r}, t)$ of electronic charge density via the Fourier series

$$\begin{aligned}\eta \Delta\rho(\mathbf{r}, t) = &\frac{\eta}{|\mathbf{a} \cdot \mathbf{b} \times \mathbf{c}|} \sum_{h,k,l} \Delta F_{hkl}(t) \\ &\times \cos[2\pi(h\,\mathbf{a}^* + k\,\mathbf{b}^* + l\,\mathbf{c}^*)\mathbf{r}].\end{aligned} \tag{3}$$

$\mathbf{a}^*$, $\mathbf{b}^*$, and $\mathbf{c}^*$ are the reciprocal lattice vectors of the lattice vectors $\mathbf{a}$, $\mathbf{b}$, and $\mathbf{c}$ of the unit cell. The spatial resolution and, thus, the accuracy of the generated electron density maps increases with the number of Debye-Scherrer rings (*hkl*) recorded up to a maximum diffraction angle θ_{max}. Deriving transient charge densities for crystalline systems without inversion symmetry requires more sophisticated methods,[55] including iterative numerical procedures such as, e.g., the Maximum Entropy Method (MEM).[92–94]

Femtosecond x-ray powder diffraction has been applied to unravel ultrafast electron relocations in the prototype transition metal complex $[Fe(bpy)_3]^{2+}$. The photophysics of the $[Fe(bpy)_3]^{2+}$ system has been studied extensively in diluted solutions by ultrafast optical spectroscopy[95] and by femtosecond x-ray absorption.[42] Optical excitation in the visible populates singlet-metal-to-ligand-charge-transfer (^{1}MCLT) states from which the system decays via several intersystem crossing steps on a sub-150 fs time scale into a high spin quintet state (^{5}T) at much lower energy. In solution, the ^{5}T state has a lifetime of approximately 600 ps. The ^{5}T state is characterized by a charge transfer from the Fe to the bpy units and, as shown by time-resolved x-ray absorption,[42,96] a lengthening of the Fe-bpy bond by 0.02 nm. In solution, the transition metal complexes and the counterions are solvated separately and the Coulomb interaction between them is negligible. In the crystalline phase with a hexagonal unit cell [Fig. 4(a)], there is a densely packaged geometry with two $(PF_6)^-$ counter ions per $[Fe(bpy)_3]^{2+}$ unit and strong Coulomb interactions between them.

In the diffraction experiments, two-photon excitation of the crystalline powder by sub-50 fs pulses at 800 nm initiated the charge transfer process and 100 fs Cu Kα pulses at 8.04 keV were diffracted from the excited powder. The diffraction pattern consisting of approximately 20 Debye-Scherrer rings displayed transient intensity changes while all angular positions remained unchanged. Electron density maps derived from the data taken at a pump-probe delay of 250 fs are shown in Fig. 4(b). The differential electron density $\eta\Delta\rho$ is projected on a plane through a PF_6^- counterion (top) and the plane of a bpy unit (bottom). The fraction of directly excited unit cells has a value of $\eta \approx 0.008$. The bottom map reveals a net electron transfer from the central Fe atom to the bpy units and an increase in the Fe-bpy distance, the latter being evident from a comparison with the contour of the unexcited system (dashed line). Surprisingly, the PF_6^- map shows a decrease of electron density which is caused by a so far unknown charge transfer from the counterions to the bpy units. To quantify the amount $\eta\Delta Q$ of transferred charge, the electron density changes were integrated over the volume of the respective unit and plotted as a function of pump-probe delay [Figs. 4(c)–4(e)]. Such transients show that the bpy ligands accept all charge transferred, with the major part coming from the counterions. The charge transfer shows a step-like time dependence which is in agreement with all-optical pump-probe studies of the crystallites[59] and with the sub-150 fs formation kinetics of the ^{5}T state in solution.

The long-range inter-ionic Coulomb interaction in the densely packed crystal is at the origin of the observed behavior. First, the electron transfer from the counterions to the bpy ligands reduces the polarity of the lattice and, thus, reduces the electrostatic energy in the crystal. Second, using a value of $\eta \approx 0.008$, one estimates a total amount $\Delta Q = 0.25/0.008 = 31.25e$ received by the bpy ligands [cf. Figs. 4(c)–4(e)]. This large value demonstrates that the charge transfer affects a much higher number of unit cells than the directly excited ones. The correlated many-body transfer of electron density

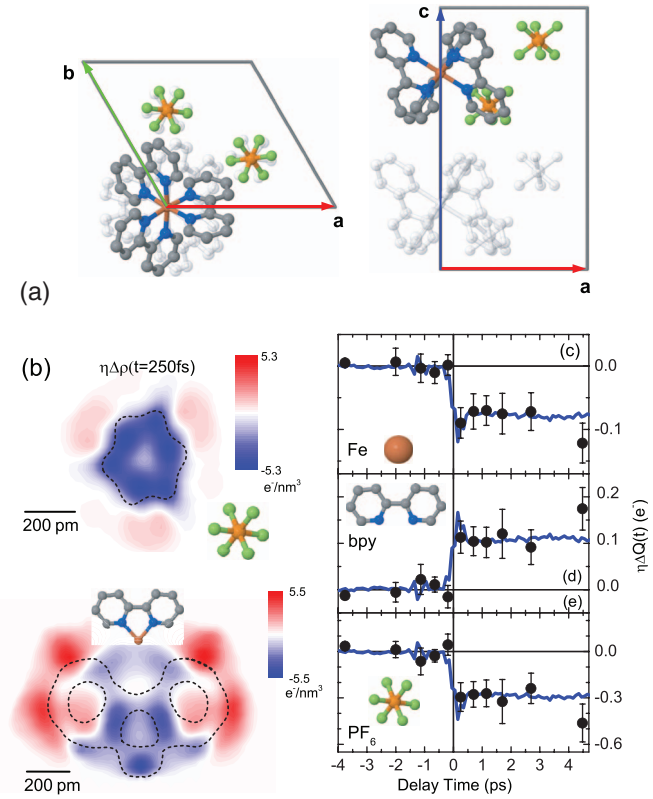

FIG. 4. (a) Unit cell of a $[Fe(bpy)_3]^{2+}(PF_6)_2$ crystal with lattice vectors **a**, **b**, and **c**. Fe atoms are shown in brown, N in blue, C in gray, F in green, and P in orange. (b) Differential electron density $\eta\Delta\rho$ at a 250 fs delay, projected on a plane through a (PF_6) counter ion and the plane of a bpy unit (η: fraction of excited unit cells). The dashed lines give the contours of the unexcited groups. ((c)–(e)) Transient change of charge $\eta\Delta Q$ integrated over the respective structural unit as a function of pump-probe delay (symbols). The charge changes show a step-like onset which is in agreement with the kinetics of optical absorption changes measured with a 400 nm pump and a 530 nm probe pulse (solid lines) and maps the formation of the long-lived spin quintet state.

is again mediated by the inner-ionic Coulomb interaction and has been analyzed in terms of electronic polaron formation in this prototype ionic material.[59] It should be noted that most applications of transition metal complexes require solid state materials for which the observed behavior is characteristic.

C. Correlated lattice, charge, and spin dynamics

The coupling between lattice, charge, and spin degrees of freedom is essential for the functional properties of a broad range of crystalline materials, in particular ionic materials and systems with correlated charge and spin systems. Very recent experiments have demonstrated that femtosecond x-ray diffraction holds a strong potential for unraveling the resulting microscopic spatio-temporal dynamics with an unprecedented specificity.

The interplay of charge and lattice degrees of freedom has been addressed in powder diffraction experiments with KH_2PO_4 (KDP), an ionic material undergoing a ferro- to paraelectric phase transition at a critical temperature $T_C = 123$ K. Electron density maps recorded in the paraelectric phase show that coherent wavepacket motions along low-frequency LO and TO phonon coordinates with a picometer spatial amplitude launch periodic charge relocations between the P and O atoms in the $H_2PO_4^-$ units over a chemical bond length of the order of 150 pm.[55] This behavior originates from the optically induced enhancement of the $H_2PO_4^-$ valence electron polarizability which makes the spatial electron distribution highly sensitive to tiny phonon elongations and results in large-amplitude charge oscillations which display decoherence times of a few picoseconds.

The strength of electron-phonon coupling in $La_{2-x}Sr_xCuO_4$, a perovskite material, has been analyzed by heating the lattice through femtosecond optical excitation and probing the angular position and intensity of the (400) Bragg peak.[97] In $La_{0.5}Sr_{1.5}MnO_4$, the lattice has been excited directly by femtosecond mid-infrared pulses and the resulting decrease of orbital and magnetic order has been followed via resonant x-ray diffraction on the Mn L_3 edge.[98] The orbital order parameter displays kinetics roughly twice as fast as the magnetic order parameter, a behavior that has been rationalized with the different symmetry of the orbitals involved in charge and spin disordering and the different charge and spin reordering processes. In the same material, the time evolution of antiferromagnetic disordering and reordering has been studied after electronic excitation.[99]

In a number of other systems, changes of spin and charge order have been induced by exciting the electronic system directly and mapped via angular position and intensity changes on individual resonant Bragg peaks. The dynamics between different spin phases of CuO has been addressed in Ref. 61. The nonequilibrium dynamics of the strongly coupled charge, orbital and spin order parameters has been studied in the stripe-ordered nickelate $La_{1.75}Sr_{0.25}NiO_4$[63,100] and in orbitally ordered thin films of $La_{0.25}Pr_{0.375}Ca_{0.375}MnO_3$[101] or $La_{0.42}Ca_{0.58}MnO_3$.[102] The results reveal a strong coupling between the two order parameters which is manifested in a similar recovery kinetics after electronic excitation. Changes of charge order connected with an insulator-metal phase transition have been elucidated in detail for the prototype material magnetite and follow a biphasic quasiparticle kinetics.[64] The interplay of chemical disorder of amorphous ferrimagnetic GdFeCo and its local dynamic magnetic properties has been elucidated in spatially resolved resonant x-ray scattering studies.[62]

IV. CONCLUSIONS AND OUTLOOK

In conclusion, ultrafast x-ray diffraction has developed into a powerful method for mapping elementary spatio-temporal dynamics in condensed matter. Recent progress in generating intense ultrashort x-ray pulses and the implementation of novel nonresonant and resonant diffraction methods has widened the scope of the field substantially, now addressing coupled nuclear motions, spatially resolved charge and spin dynamics and reversible phase transitions in crystalline materials. In particular, the coupling of different types of elementary excitations has become an important topic and highly specific x-ray probes are at hand to disentangle the resulting highly complex dynamics.

There are ongoing strong efforts to further improve the sources of ultrashort x-ray pulses. Seeding of FELs will

provide intense coherent soft and hard x-ray pulses that should pave the way towards nonlinear x-ray optics, in particular coherent nonlinear spectroscopy and imaging. An improved synchronization of FELs with optical sources will allow for a 10 fs time resolution of pump-probe experiments. An important trend in the development of laser-driven sources is intense mid-infrared drivers working at kilohertz repetition rates which will enable a much higher hard x-ray flux from plasma sources. This will be essential for reducing measurement times and for increasing the high sensitivity of diffraction experiments with such sources even further. Novel laser-based sources will also play a key role in developing new and much more specific optical excitation schemes to initiate structural dynamics. Ultrashort terahertz transients with field amplitudes up to MV/cm are important for studying field induced processes and structural dynamics in electronic ground states while excitation schemes with tailored sequences of pulses will allow for driving vibrational and electronic coherences with large amplitudes. Such technological progress should allow for addressing structural dynamics in complex systems with much larger polyatomic unit cells, including crystallized macromolecular systems.

ACKNOWLEDGMENTS

We thank Klaus Sokolowski-Tinten, Universität Duisburg-Essen, for providing Figure 2 and for valuable discussions. Part of the research at the Max-Born-Institute has received funding from the European Research Council under the European Union's Seventh Framework Programme (FP7/2007-2012)/ERC Grant Agreement No. 247051 and from the Deutsche Forschungsgemeinschaft (Grant No. WO 558/13-1).

[1] *XVIIIth International Conference on Ultrafast Phenomena*, edited by M. Chergui, A. Taylor, S. Cundiff, R. de Vivie-Riedle, and K. Yamagouchi, EPJ Web of Conferences Vol. 41 (EDP Sciences, Les Ulis, 2013).
[2] A. Rousse, C. Rischel, and J. Gauthier, Rev. Mod. Phys. **73**, 17 (2001).
[3] D. von der Linde, K. Sokolowski-Tinten, C. Blome, C. Dietrich, A. Tarasevitch, A. Cavalleri, and J. A. Squier, Z. Phys. Chem. **215**, 1527 (2001).
[4] M. Bargheer, N. Zhavoronkov, M. Woerner, and T. Elsaesser, Chem. Phys. Chem. **7**, 783 (2006).
[5] M. Chergui and A. H. Zewail, Chem. Phys. Chem. **10**, 28 (2009).
[6] G. Sciaini and R. J. D. Miller, Rep. Prog. Phys. **74**, 096101 (2011).
[7] C. Bostedt, J. D. Bozek, P. H. Bucksbaum, R. N. Coffee, J. B. Hastings, Z. Huang, R. W. Lee, S. Schorb, J. N. Corlett, P. Denes, P. Emma, R. W. Falcone, R. W. Schoenlein, G. Doumy, E. P. Kanter, B. Kraessig, S. Southworth, L. Young, L. Fang, M. Hoener, N. Berrah, C. Roedig, and L. F. DiMauro, J. Phys. B **46**, 164003 (2013).
[8] M. Hada, K. Pichugin, and G. Sciaini, Eur. Phys. J. Spec. Top. **222**, 1093 (2013).
[9] C. Barty, M. Ben-Nun, T. Guo, F. Raksi, C. Rose-Petruck, J. Squier, K. R. Wilson, V. V. Yakovlev, P. M. Weber, Z. Jiang, A. Ikhlef, and J.-C. Kieffer, *in Time-Resolved Diffraction*, edited by J. Helliwell and P. M. Rentzepis (Oxford University Press, New York, 1998).
[10] C. v. Korff Schmising, M. Bargheer, M. Woerner, and T. Elsaesser, Z. Kristallogr. **223**, 283 (2008).
[11] T. Elsaesser and M. Woerner, Acta Crystallogr. A **66**, 168 (2010).
[12] H. N. Chapman, P. Fromme, A. Barty, T. A. White, R. A. Kirian, A. Aquila, M. S. Hunter, J. Schulz, D. P. DePonte, U. Weierstall, R. B. Doak, F. R. N. C. Maia, A. V. Martin, I. Schlichting, L. Lomb, N. Coppola, R. L. Shoeman, S. W. Epp, R. Hartmann, D. Rolles, A. Rudenko, L. Foucar, N. Kimmel, G. Weidenspointner, P. Holl, M. Liang, M. Barthelmess, C. Caleman, S. Boutet, M. J. Bogan, J. Krzywinski, C. Bostedt, S. Bajt, L. Gumprecht, B. Rudek, B. Erk, C. Schmidt, A. Hömke, C. Reich, D. Pietschner, L. Strüder, G. Hauser, H. Gorke, J. Ullrich, S. Herrmann, G. Schaller, F. Schopper, H. Soltau, K.-U. Kühnel, M. Messerschmidt, J. D. Bozek, S. P. Hau-Riege, M. Frank, C. Y. Hampton, R. G. Sierra, D. Starodub, G. J. Williams, J. Hajdu, N. Timneanu, M. M. Seibert, J. Andreasson, A. Rocker, O. Jönsson, M. Svenda, S. Stern, K. Nass, R. Andritschke, C.-D. Schröter, F. Krasniqi, M. Bott, K. E. Schmidt, X. Wang, I. Grotjohann, J. M. Holton, T. R. M. Barends, R. Neutze, S. Marchesini, R. Fromme, S. Schorb, D. Rupp, M. Adolph, T. Gorkhover, I. Andersson, H. Hirsemann, G. Potdevin, H. Graafsma, B. Nilsson, and J. C. H. Spence, Nature **470**, 73 (2011).
[13] J. Kern, R. Alonso-Mori, J. Hellmich, R. Tran, J. Hattne, H. Laksmono, C. Glöckner, N. Echols, R. G. Sierra, J. Sellberg, B. Lassalle-Kaiser, R. J. Gildea, P. Glatzel, R. W. Grosse-Kunstleve, M. J. Latimer, T. A. McQueen, D. DiFiore, A. R. Fry, M. Messerschmidt, A. Miahnahri, D. W. Schafer, M. M. Seibert, D. Sokaras, T.-C. Weng, P. H. Zwart, W. E. White, P. D. Adams, M. J. Bogan, S. Boutet, G. J. Williams, J. Messinger, N. K. Sauter, A. Zouni, U. Bergmann, J. Yano, and V. K. Yachandra, Proc. Natl. Acad. Sci. U.S.A. **109**, 9721 (2012).
[14] S. Khan, J. Mod. Opt. **55**, 3469 (2008).
[15] V. Ayvazyan, N. Baboi, J. Bähr, V. Balandin, B. Beutner, A. Brandt, I. Bohnet, A. Bolzmann, R. Brinkmann, O. I. Brovko, J. P. Carneiro, S. Casalbuoni, M. Castellano, P. Castro, L. Catani, E. Chiadroni, S. Choroba, A. Cianchi, H. Delsim-Hashemi, G. Di Pirro, M. Dohlus, S. Düsterer, H. T. Edwards, B. Faatz, A. A. Fateev, J. Feldhaus, K. Flöttmann, J. Frisch, L. Fröhlich, T. Garvey, U. Gensch, N. Golubeva, H.-J. Grabosch, B. Grigoryan, O. Grimm, U. Hahn, J. H. Han, M. V. Hartrott, K. Honkavaara, M. Hüning, R. Ischebeck, E. Jaeschke, M. Jablonka, R. Kammering, V. Katalev, B. Keitel, S. Khodyachykh, Y. Kim, V. Kocharyan, M. Körfer, M. Kollewe, D. Kostin, D. Krämer, M. Krassilnikov, G. Kube, L. Lilje, T. Limberg, D. Lipka, F. Löhl, M. Luong, C. Magne, J. Menzel, P. Michelato, V. Miltchev, M. Minty, W. D. Möller, L. Monaco, W. Müller, M. Nagl, O. Napoly, P. Nicolosi, D. Nölle, T. Nunez, A. Oppelt, C. Pagani, R. Paparella, B. Petersen, B. Petrosyan, J. Pflüger, P. Piot, E. Plönjes, L. Poletto, D. Proch, D. Pugachov, K. Rehlich, D. Richter, S. Riemann, M. Ross, J. Rossbach, M. Sachwitz, E. L. Saldin, W. Sandner, H. Schlarb, B. Schmidt, M. Schmitz, P. Schmüser, J. R. Schneider, E. A. Schneidmiller, H.-J. Schreiber, S. Schreiber, A. V. Shabunov, D. Sertore, S. Setzer, S. Simrock, E. Sombrowski, L. Staykov, B. Steffen, F. Stephan, F. Stulle, K. P. Sytchev, H. Thom, K. Tiedtke, M. Tischer, R. Treusch, D. Trines, I. Tsakov, A. Vardanyan, R. Wanzenberg, T. Weiland, H. Weise, M. Wendt, I. Will, A. Winter, K. Wittenburg, M. V. Yurkov, I. Zagorodnov, P. Zambolin, and K. Zapfe, Eur. Phys. J. D **37**, 297 (2006).
[16] P. Emma, R. Akre, J. Arthur, R. Bionta, C. Bostedt, J. Bozek, A. Brachmann, P. Bucksbaum, R. Coffee, F.-J. Decker, Y. Ding, D. Dowell, S. Edstrom, A. Fisher, J. Frisch, S. Gilevich, J. Hastings, G. Hays, P. Hering, Z. Huang, R. Iverson, H. Loos, M. Messerschmidt, A. Miahnahri, S. Moeller, H.-D. Nuhn, G. Pile, D. Ratner, J. Rzepiela, D. Schultz, T. Smith, P. Stefan, H. Tompkins, J. Turner, J. Welch, W. White, J. Wu, G. Yocky, and J. Galayda, Nature Photon. **4**, 641 (2010).
[17] T. Ishikawa, H. Aoyagi, T. Asaka, Y. Asano, N. Azumi, T. Bizen, H. Ego, K. Fukami, T. Fukui, Y. Furukawa, S. Goto, H. Hanaki, T. Hara, T. Hasegawa, T. Hatsui, A. Higashiya, T. Hirono, N. Hosoda, M. Ishii, T. Inagaki, Y. Inubushi, T. Itoga, Y. Joti, M. Kago, T. Kameshima, H. Kimura, Y. Kirihara, A. Kiyomichi, T. Kobayashi, C. Kondo, T. Kudo, H. Maesaka, X. M. Maréchal, T. Masuda, S. Matsubara, T. Matsumoto, T. Matsushita, S. Matsui, M. Nagasono, N. Nariyama, H. Ohashi, T. Ohata, T. Ohshima, S. Ono, Y. Otake, C. Saji, T. Sakurai, T. Sato, K. Sawada, T. Seike, K. Shirasawa, T. Sugimoto, S. Suzuki, S. Takahashi, H. Takebe, K. Takeshita, K. Tamasaku, H. Tanaka, R. Tanaka, T. Tanaka, T. Togashi, K. Togawa, A. Tokuhisa, H. Tomizawa, K. Tono, S. Wu, M. Yabashi, M. Yamaga, A. Yamashita, K. Yanagida, C. Zhang, T. Shintake, H. Kitamura, and N. Kumagai, Nature Photon. **6**, 540 (2012).
[18] S. Lee, W. Roseker, C. Gutt, Z. Huang, Y. Ding, G. Grübel, and A. Robert, Opt. Express **20**, 9790 (2012).
[19] I. A. Vartanyants, A. Singer, A. P. Mancuso, O. M. Yefanov, A. Sakdinawat, Y. Liu, E. Bang, G. J. Williams, G. Cadenazzi, B. Abbey, H. Sinn, D. Attwood, K. A. Nugent, E. Weckert, T. Wang, D. Zhu, B. Wu, C. Graves, A. Scherz, J. J. Turner, W. F. Schlotter, M. Messerschmidt, J. Lüning, Y. Acremann, P. Heimann, D. C. Mancini, V. Joshi, J. Krzywinski, R. Soufli, M. Fernandez-Perea, S. Hau-Riege, A. G. Peele, Y. Feng, O. Krupin, S. Moeller, and W. Wurth, Phys. Rev. Lett. **107**, 144801 (2011).
[20] J. Amann, W. Berg, V. Blank, F.-J. Decker, Y. Ding, P. Emma, Y. Feng, J. Frisch, D. Fritz, J. Hastings, Z. Huang, J. Krzywinski, R. Lindberg,

H. Loos, A. Lutman, H.-D. Nuhn, D. Ratner, J. Rzepiela, D. Shu, Yu. Shvyd'ko, S. Spampinati, S. Stoupin, S. Terentyev, E. Trakhtenberg, D. Walz, J. Welch, J. Wu, A. Zholents, and D. Zhu, Nature Photon. **6**, 693 (2012).
[21]E. Allaria, R. Appio, L. Badano, W. A. Barletta, S. Bassanese, S. G. Biedron, A. Borga, E. Busetto, D. Castronovo, P. Cinquegrana, S. Cleva, D. Cocco, M. Cornacchia, P. Craievich, I. Cudin, G. D'Auria, M. Dal Forno, M. B. Danailov, R. De Monte, G. De Ninnol, P. Delgiusto, A. Demidovich, S. Di Mitri, B. Diviacco, A. Fabris, R. Fabris, W. Fawley, M. Ferianis, E. Ferrari, S. Ferry, L. Froehlich, P. Furlan, G. Gaio, F. Gelmetti, L. Giannessi, M. Giannini, R. Gobessi, R. Ivanov, E. Karantzoulis, M. Lonza, A. Lutman, B. Mahieu, M. Milloch, S. V. Milton, M. Musardo, I. Nikolov, S. Noe, F. Parmigiani, G. Penco, M. Petronio, L. Pivetta, M. Predonzani, F. Rossi, L. Rumiz, A. Salom, C. Scafuri, C. Serpico, P. Sigalotti, S. Spampinati, C. Spezzani, M. Svandrlik, C. Svetina, S. Tazzari, M. Trovo, R. Umer, A. Vascotto, M. Veronese, R. Visintini, M. Zaccaria, D. Zangrando, and M. Zangrando, Nature Photon. **6**, 699 (2012).
[22]R. W. Schoenlein, W. P. Leemans, A. H. Chin, P. Volfbeyn, T. E. Glover, P. Balling, M. Zolotorev, K.-J. Kim, S. Chattopadhyay, and C. V. Shank, Science **274**, 236 (1996).
[23]S. Khan, K. Holldack, T. Kachel, R. Mitzner, and T. Quast, Phys. Rev. Lett. **97**, 074801 (2006).
[24]P. Beaud, S. L. Johnson, A. Streun, R. Abela, D. Abramsohn, D. Grolimund, F. Krasniqi, T. Schmidt, V. Schlott, and G. Ingold, Phys. Rev. Lett. **99**, 174801 (2007).
[25]D. Kmetec, C. L. Gordon III, J. J. Macklin, B. E. Lemoff, G. S. Brown, and S. E. Harris, Phys. Rev. Lett. **68**, 1527 (1991).
[26]M. M. Murnane, H. C. Kapteyn, M. D. Rosen, and R. W. Falcone, Science **251**, 531 (1991).
[27]F. Brunel, Phys. Rev. Lett. **59**, 52 (1987).
[28]G. Korn, A. Thoss, H. Stiel, U. Vogt, M. Richardson, T. Elsaesser, and M. Faubel, Opt. Lett. **27**, 866 (2002).
[29]Y. Jiang, T. Lee, W. Li, G. Ketwaroo, and C. G. Rose-Petruck, Opt. Lett. **27**, 963 (2002).
[30]N. Zhavoronkov, Y. Gritsai, M. Bargheer, M. Woerner, T. Elsaesser, F. Zamponi, I. Uschmann, and E. Förster, Opt. Lett. **30**, 1737 (2005).
[31]F. Zamponi, Z. Ansari, C. Korff v. Schmising, P. Rothhardt, N. Zhavoronkov, M. Woerner, T. Elsaesser, M. Bargheer, T. Trobitzsch-Ryll, and M. Haschke, Appl. Phys. A **96**, 51 (2009).
[32]A. L. Cavalieri, D. M. Fritz, S. H. Lee, P. H. Bucksbaum, D. A. Reis, J. Rudati, D. M. Mills, P. H. Fuoss, G. B. Stephenson, C. C. Kao, D. P. Siddons, D. P. Lowney, A. G. MacPhee, D. Weinstein, R. W. Falcone, R. Pahl, J. Als-Nielsen, C. Blome, S. Düsterer, R. Ischebeck, H. Schlarb, H. Schulte-Schrepping, Th. Tschentscher, J. Schneider, O. Hignette, F. Sette, K. Sokolowski-Tinten, H. N. Chapman, R. W. Lee, T. N. Hansen, O. Synnergren, J. Larsson, S. Techert, J. Sheppard, J. S. Wark, M. Bergh, C. Caleman, G. Huldt, D. van der Spoel, N. Timneanu, J. Hajdu, R. A. Akre, E. Bong, P. Emma, P. Krejcik, J. Arthur, S. Brennan, K. J. Gaffney, A. M. Lindenberg, K. Luening, and J. B. Hastings, Phys. Rev. Lett. **94**, 114801 (2005).
[33]F. Löhl, V. Arsov, M. Felber, K. Hacker, W. Jalmuzna, B. Lorbeer, F. Ludwig, K.-H. Matthiesen, H. Schlarb, B. Schmidt, P. Schmüser, S. Schulz, J. Szewinski, A. Winter, and J. Zemella, Phys. Rev. Lett. **104**, 144801 (2010).
[34]T. Maltezopoulos, S. Cunovic, M. Wieland, M. Beye, A. Azima, H. Redlin, M. Krikunova, R. Kalms, U. Frühling, F. Budzyn, W. Wurth, A. Föhlisch, and M. Drescher, New J. Phys. **10**, 033026 (2008).
[35]A. Azima, S. Düsterer, P. Radcliffe, H. Redlin, N. Stojanovic, W. Li, H. Schlatb, J. Feldhaus, D. Cubaynes, M. Meyer, J. Dardis, P. Hayden, P. Hough, V. Richardson, E. T. Kennedy, and J. T. Costello, Appl. Phys. Lett. **94**, 144102 (2009).
[36]F. Tavella, N. Stojanovic, G. Geloni, and M. Gensch, Nature Photon. **5**, 162 (2011).
[37]O. Krupin, M. Trigo, W. F. Schlotter, M. Beye, F. Sorgenfrei, J. J. Turner, D. A. Reis, N. Gerken, S. Lee, W. S. Lee, G. Hays, Y. Acremann, B. Abbey, R. Coffee, M. Messerschmidt, S. P. Hau-Riege, G. Lapertot, J. Lüning, P. Heimann, R. Soufli, M. Fernández-Perea, M. Rowen, M. Holmes, S. L. Molodtsov, A. Föhlisch, and W. Wurth, Opt. Express **20**, 11396 (2012).
[38]M. Harmand, R. Coffee, M. R. Bionta, M. Chollet, D. French, D. Zhu, D. M. Fritz, H. T. Lemke, N. Medvedev, B. Ziaja, S. Toleikis, and M. Cammarata, Nature Photon. **7**, 215 (2013).
[39]C. Bressler and M. Chergui, Chem. Rev. **104**, 1781 (2004).
[40]L. X. Chen, Annu. Rev. Phys. Chem. **56**, 221 (2005).
[41]M. Chergui, Acta Crystallogr. **A66**, 229 (2010).
[42]C. Bressler, C. J. Milne, V.-T. Pham, A. ElNahhas, R. M. van der Veen, W. Gawelda, S. L. Johnson, P. Beaud, D. Grolimund, M. Kaiser, C. N. Borca, G. Ingold, R. Abela, and M. Chergui, Science **323**, 489 (2009).
[43]H. T. Lemke, C. Bressler, L. X. Chen, D. M. Fritz, K. J. Gaffney, A. Galler, W. Gawelda, K. Haldrup, R. W. Hartsock, H. Ihee, J. Kim, K. H. Kim, J. H. Lee, M. M. Nielsen, A. B. Stickrath, W. Zhang, D. Zhu, and M. Cammarata, J. Phys. Chem. A **117**, 735 (2013).
[44]K. Sokolowski-Tinten, C. Blome, J. Blums, A. Cavalleri, C. Dietrich, A. Tarasevitch, I. Uschmann, E. Förster, M. Kammler, M. Horn-von-Hoegen, and D. von der Linde, Nature **422**, 287 (2003).
[45]M. Bargheer, N. Zhavoronkov, Y. Gritsai, J. C. Woo, D. S. Kim, M. Woerner, and T. Elsaesser, Science **306**, 1771 (2004).
[46]A. Cavalleri, S. Wall, C. Simpson, E. Statz, D. W. Ward, K. A. Nelson, M. Rini, and R. W. Schoenlein, Nature **442**, 664 (2006).
[47]M. Bargheer, N. Zhavoronkov, R. Bruch, H. Legall, H. Stiel, M. Woerner, and T. Elsaesser, Appl. Phys. B **80**, 715 (2005).
[48]M. Braun, C. v. Korff-Schmising, M. Kiel, N. Zhavoronkov, J. Dreyer, M. Bargheer, T. Elsaesser, C. Root, T. E. Schrader, P. Gilch, W. Zinth, and M. Woerner, Phys. Rev. Lett. **98**, 248301 (2007).
[49]D. M. Fritz, D. A. Reis, B. Adams, R. A. Akre, J. Arthur, C. Blome, P. H. Bucksbaum, A. L. Cavalieri, S. Engemann, S. Fahy, R. W. Falcone, P. H. Fuoss, K. J. Gaffney, M. J. George, J. Hajdu, M. P. Hertlein, P. B. Hillyard, M. Horn-von Hoegen, M. Kammler, J. Kaspar, R. Kienberger, P. Krejcik, S. H. Lee, A. M. Lindenberg, B. McFarland, D. Meyer, T. Montagne, É. D. Murray, A. J. Nelson, M. Nicoul, R. Pahl, J. Rudati, H. Schlarb, D. P. Siddons, K. Sokolowski-Tinten, Th. Tschentscher, D. von der Linde, and J. B. Hastings, Science **315**, 633 (2007).
[50]M. Braun, C. Root, F. J. Lederer, T. E. Schrader, W. Zinth, C. von Korff Schmising, M. Bargheer, T. Elsaesser, and M. Woerner, Appl. Phys. A **96**, 107 (2009).
[51]S. L. Johnson, E. Vorobeva, P. Beaud, C. J. Milne, and G. Ingold, Phys. Rev. Lett. **103**, 205501 (2009).
[52]B. Freyer, J. Stingl, F. Zamponi, M. Woerner, and T. Elsaesser, Opt. Express **19**, 15506 (2011).
[53]F. Zamponi, Z. Ansari, M. Woerner, and T. Elsaesser, Opt. Express **18**, 947 (2010).
[54]M. Woerner, F. Zamponi, Z. Ansari, J. Dreyer, B. Freyer, M. Prémont-Schwarz, and T. Elsaesser, J. Chem. Phys. **133**, 064509 (2010).
[55]F. Zamponi, P. Rothhardt, J. Stingl, M. Woerner, and T. Elsaesser, Proc. Natl. Acad. Sci. U.S.A. **109**, 5207 (2012).
[56]F. Zamponi, J. Stingl, M. Woerner, and T. Elsaesser, Phys. Chem. Chem. Phys. **14**, 6156 (2012).
[57]J. Stingl, F. Zamponi, B. Freyer, M. Woerner, T. Elsaesser, and A. Borgschulte, Phys. Rev. Lett. **109**, 147402 (2012).
[58]V. Juvé, M. Holtz, F. Zamponi, M. Woerner, T. Elsaesser, and A. Borgschulte, Phys. Rev. Lett. **111**, 217401 (2013).
[59]B. Freyer, F. Zamponi, V. Juvé, J. Stingl, M. Woerner, T. Elsaesser, and M. Chergui, J. Chem. Phys. **138**, 144504 (2013).
[60]J.-L. Hodeau, V. Favre-Nicolin, S. Bos, H. Renevier, E. Lorenzo, and J.-F. Berar, Chem. Rev. **101**, 1843 (2001).
[61]S. L. Johnson, R. A. de Souza, U. Staub, P. Beaud, E. Möhr-Vorobeva, G. Ingold, A. Caviezel, V. Scagnoli, W. F. Schlotter, J. J. Turner, O. Krupin, W.-S. Lee, Y.-D. Chuang, L. Patthey, R. G. Moore, D. Lu, M. Yi, P. S. Kirchmann, M. Trigo, P. Denes, D. Doering, Z. Hussain, Z.-X. Shen, D. Prabhakaran, and A. T. Boothroyd, Phys. Rev. Lett. **108**, 037203 (2012).
[62]C. E. Graves, A. H. Reid, T. Wang, B. Wu, S. de Jong, K. Vahaplar, I. Radu, D. P. Bernstein, M. Messerschmidt, L. Müller, R. Coffee, M. Bionta, S. W. Epp, R. Hartmann, N. Kimmel, G. Hauser, A. Hartmann, P. Holl, H. Gorke, J. H. Mentink, A. Tsukamoto, A. Fognini, J. J. Turner, W. F. Schlotter, D. Rolles, H. Soltau, L. Strüder, Y. Acremann, A. V. Kimel, A. Kirilyuk, T. Rasing, J. Stöhr, A. O. Scherz, and H. A. Dürr, Nature Mater. **12**, 293 (2013).
[63]Y. D. Chuang, W. S. Lee, Y. F. Kung, A. P. Sorini, B. Moritz, R. G. Moore, L. Patthey, M. Trigo, D. H. Lu, P. S. Kirchmann, M. Yi, O. Krupin, M. Langner, Y. Zhu, S. Y. Zhou, D. A. Reis, N. Huse, J. S. Robinson, R. A. Kaindl, R. W. Schoenlein, S. L. Johnson, M. Först, D. Doering, P. Denes, W. F. Schlotter, J. J. Turner, T. Sasagawa, Z. Hussain, Z. X. Shen, and T. P. Devereaux, Phys. Rev. Lett. **110**, 127404 (2013).
[64]S. de Jong, R. Kukreja, C. Trabant, N. Pontius, C. F. Chang, T. Kachel, M. Beye, F. Sorgenfrei, C. H. Back, B. Bräuer, W. F. Schlotter, J. J. Turner, O. Krupin, M. Doehler, D. Zhu, M. A. Hossain, A. O. Scherz, D. Fausti, F. Novelli, M. Esposito, W. S. Lee, Y. D. Chuang, D. H. Lu, R. G. Moore, M. Yi, M. Trigo, P. Kirchmann, L. Pathey, M. S. Golden, M. Buchholz,

P. Metcalf, F. Parmigiani, W. Wurth, A. Föhlisch, C. Schüssler-Langeheine, and H. A. Dürr, Nature Mater. **12**, 882 (2013).
[65]A. M. Lindenberg, I. Kang, S. L. Johnson, T. Missalla, P. A. Heimann, Z. Chang, J. Larsson, P. H. Bucksbaum, H. C. Kapteyn, H. A. Padmore, R. W. Lee, J. S. Wark, and R. W. Falcone, Phys. Rev. Lett. **84**, 111 (2000).
[66]M. Först and T. Dekorsy, in *Coherent Vibrational Dynamics*, edited by S. DeSilvestri, G. Cerullo, and G. Lanzano (CRC Press (Taylor and Francis Group), London, 2008), p. 129.
[67]M. Bargheer, N. Zhavoronkov, J. C. Woo, D. S. Kim, M. Woerner, and T. Elsaesser, Phys. Status Solidi B **243**, 2389 (2006).
[68]S. Y. Lee and E. J. Heller, J. Chem. Phys. **71**, 4777 (1979).
[69]T. E. Stevens, J. Kuhl, and R. Merlin, Phys. Rev. B **65**, 144304 (2002).
[70]W. Lu, M. Nicoul, U. Shymanovich, A. Tarasevitch, M. Kammler, M. H. von Hoegen, D. von der Linde, and K. Sokolowski-Tinten, Mater. Res. Soc. Symp. Proc. **1230**, MM03 (2010).
[71]S. L. Johnson, P. Beaud, C. J. Milne, F. S. Krasniqi, E. S. Zijlstra, M. E. Garcia, M. Kaiser, D. Grolimund, R. Abela, and G. Ingold, Phys. Rev. Lett. **100**, 155501 (2008).
[72]S. L. Johnson, P. Beaud, E. Vorobeva, C. J. Milne, E. D. Murray, S. Fahy, and G. Ingold, Phys. Rev. Lett. **102**, 175503 (2009).
[73]Y. Giret, A. Gellé, and B. Arnaud, Phys. Rev. Lett. **106**, 155503 (2011).
[74]S. L. Johnson, P. Beaud, E. Möhr-Vorobeva, A. Caviezel, G. Ingold, and C. J. Milne, Phys. Rev. B **87**, 054301 (2013).
[75]E. D. Murray, S. Fahy, D. Prendergast, T. Ogitsu, D. M. Fritz, and D. A. Reis, Phys. Rev. B **75**, 184301 (2007).
[76]C. Colvard, T. A. Gant, M. V. Klein, R. Merlin, R. Fischer, H. Morkoc, and A. C. Gossard, Phys. Rev. B **31**, 2080 (1985).
[77]C. v. Korff Schmising, A. Harpoeth, N. Zhavoronkov, Z. Ansari, C. Aku-Leh, M. Woerner, T. Elsaesser, M. Bargheer, M. Schmidbauer, I. Vrejoiu, D. Hesse, and M. Alexe, Phys. Rev. B **78**, 060404(R) (2008).
[78]C. v. Korff Schmising, M. Bargheer, M. Kiel, N. Zhavoronkov, M. Woerner, T. Elsaesser, I. Vrejoiu, D. Hesse, and M. Alexe, Phys. Rev. B **73**, 212202 (2006).
[79]C. v. Korff Schmising, M. Bargheer, M. Kiel, N. Zhavoronkov, M. Woerner, T. Elsaesser, M. Bargheer, I. Vrejoiu, D. Hesse, and M. Alexe, Phys. Rev. Lett. **98**, 257601 (2007).
[80]M. Woerner, C. v. Korff Schmising, M. Bargheer, N. Zhavoronkov, I. Vrejoiu, D. Hesse, M. Alexe, and T. Elsaesser, Appl. Phys. A **96**, 83 (2009).
[81]C. v. Korff Schmising, A. Harpoeth, N. Zhavoronkov, M. Woerner, T. Elsaesser, M. Bargheer, M. Schmidbauer, I. Vrejoiu, D. Hesse, and M. Alexe, Phys. Proc. **3**, 333 (2010).
[82]D. Schick, A. Bojahr, M. Herzog, C. von Korff Schmising, R. Shayduk, W. Leitenberger, P. Gaal, and M. Bargheer, Rev. Sci. Instrum. **83**, 025104 (2012).
[83]A. Bojahr, D. Schick, L. Maerten, M. Herzog, I. Vrejoiu, C. von Korff Schmising, C. Milne, S. L. Johnson, and M. Bargheer, Phys. Rev. B **85**, 224302 (2012).
[84]R. Shayduk, M. Herzog, A. Bojahr, D. Schick, P. Gaal, W. Leitenberger, H. Navirian, M. Sander, J. Goldshteyn, I. Vrejoiu, and M. Bargheer, Phys. Rev. B **87**, 184301 (2013).
[85]D. Schick, A. Bojahr, M. Herzog, P. Gaal, I. Vrejoiu, and M. Bargheer, Phys. Rev. Lett. **110**, 095502 (2013).
[86]A. M. Lindenberg, J. Larsson, K. Sokolowski-Tinten, K. J. Gaffney, C. Blome, O. Synnergren, J. Sheppard, C. Caleman, A. G. MacPhee, D. Weinstein, D. P. Lowney, T. K. Allison, T. Matthews, R. W. Falcone, A. L. Cavalieri, D. M. Fritz, S. H. Lee, P. H. Bucksbaum, D. A. Reis, J. Rudati, P. H. Fuoss, C. C. Kao, D. P. Siddons, R. Pahl, J. Als-Nielsen, S. Duesterer, R. Ischebeck, H. Schlarb, H. Schulte-Schrepping, T. Tschentscher, J. Schneider, D. von der Linde, O. Hignette, F. Sette, H. N. Chapman, R. W. Lee, T. N. Hansen, S. Techert, J. S. Wark, M. Bergh, G. Huldt, D. van der Spoel, N. Timneanu, J. Hajdu, R. A. Akre, E. Bong, P. Krejcik, J. Arthur, S. Brennan, K. Luening, and J. B. Hastings, Science **308**, 392 (2005).
[87]K. J. Gaffney, A. M. Lindenberg, J. Larsson, K. Sokolowski-Tinten, C. Blome, O. Synnergren, J. Sheppard, C. Caleman, A. G. MacPhee, D. Weinstein, D. P. Lowney, T. Allison, T. Matthews, R. W. Falcone, A. L. Cavalieri, D. M. Fritz, S. H. Lee, P. H. Bucksbaum, D. A. Reis, J. Rudati, A. T. Macrander, P. H. Fuoss, C. C. Kao, D. P. Siddons, R. Pahl, K. Moffat, J. Als-Nielsen, S. Duesterer, R. Ischebeck, H. Schlarb, H. Schulte-Schrepping, J. Schneider, D. von der Linde, O. Hignette, F. Sette, H. N. Chapman, R. W. Lee, T. N. Hansen, J. S. Wark, M. Bergh, G. Huldt, D. van der Spoel, N. Timneanu, J. Hajdu, R. A. Akre, E. Bong, P. Krejcik, J. Arthur, S. Brennan, K. Luening, and J. B. Hastings, Phys. Rev. Lett. **95**, 125701 (2005).
[88]H. Enquist, H. Navirian, T. N. Hansen, A. M. Lindenberg, P. Sondhauss, O. Synnergren, J. S. Wark, and J. Larsson, Phys. Rev. Lett. **98**, 225502 (2007).
[89]E. S. Zijlstra, J. Walkenhorst, and M. E. Garcia, Phys. Rev. Lett. **101**, 135701 (2008).
[90]P. Coppens, *X-Ray Charge Densities and Chemical Bonding* (Oxford University Press, 1997).
[91]J. Drenth, *Principles of Protein X-Ray Crystallography* (Springer, New York, 1999).
[92]E. Jaynes, Phys. Rev. **108**, 171 (1957).
[93]C. Gilmore, Acta Crystallogr. **A52**, 561 (1996).
[94]S. Smaalen, L. Palatinus, and M. Schneider, Acta Crystallogr. **A59**, 459 (2003).
[95]A. Canizzo, C. J. Milne, C. Consani, W. Gawelda, C. Bressler, F. van Mourik, and M. Chergui, Coord. Chem. Rev. **254**, 2677 (2010).
[96]W. Gawelda, V.-T. Pham, M. Benfatto, Y. Zaushitsyn, M. Kaiser, D. Grolimund, S. L. Johnson, R. Abela, A. Hauser, C. Bressler, and M. Chergui, Phys. Rev. Lett. **98**, 057401 (2007).
[97]B. Mansart, M. J. G. Cottet, G. F. Mancini, T. Jarlborg, S. B. Dugdale, S. L. Johnson, S. O. Mariager, C. J. Milne, P. Beaud, S. Grübel, J. A. Johnson, T. Kubacka, G. Ingold, K. Prsa, H. M. Ronnow, K. Conder, E. Pomjakushina, M. Chergui, and F. Carbone, Phys. Rev. B **88**, 054507 (2013).
[98]M. Först, R. I. Tobey, S. Wall, H. Bromberger, V. Khanna, A. L. Cavalieri, Y.-D. Chuang, W. S. Lee, R. Moore, W. F. Schlotter, J. J. Turner, O. Krupin, M. Trigo, H. Zheng, J. F. Mitchell, S. S. Dhesi, J. P. Hill, and A. Cavalleri, Phys. Rev. B **84**, 241104(R) (2011).
[99]R. I. Tobey, S. Wall, M. Först, H. Bromberger, V. Khanna, J. J. Turner, W. Schlotter, M. Trigo, O. Krupin, W. S. Lee, Y.-D. Chuang, R. Moore, A. L. Cavalieri, S. B. Wilkins, H. Zheng, J. F. Mitchell, S. S. Dhesi, A. Cavalleri, and J. P. Hill, Phys. Rev. B **86**, 064425 (2012).
[100]W. S. Lee, Y. D. Chuang, R. G. Moore, Y. Zhu, L. Patthey, M. Trigo, D. H. Lu, P. S. Kirchmann, O. Krupin, M. Yi, M. Langner, N. Huse, J. S. Robinson, Y. Chen, S. Y. Zhou, G. Coslovich, B. Huber, D. A. Reis, R. A. Kaindl, R. W. Schoenlein, D. Doering, P. Denes, W. F. Schlotter, J. J. Turner, S. L. Johnson, M. Först, T. Sasagawa, Y. F. Kung, A. P. Sorini, A. F. Kemper, B. Moritz, T. P. Devereaux, D.-H. Lee, Z. X. Shen, and Z. Hussain, Nature Commun. **3**, 838 (2012).
[101]P. Beaud, S. L. Johnson, E. Vorobeva, U. Staub, R. A. De Souza, C. J. Milne, Q. X. Jia, and G. Ingold, Phys. Rev. Lett. **103**, 155702 (2009).
[102]A. Caviezel, S. O. Mariager, S. L. Johnson, E. Möhr-Vorobeva, S. W. Huang, G. Ingold, U. Staub, C. J. Milne, S.-W. Cheong, and P. Beaud, Phys. Rev. B **87**, 205104 (2013).